Electron conic distributions produced by solar ionizing radiation

W.K. Peterson[1], Bill.Peterson@lasp.colorado.edu, 1-303-492-0608, FAX: none

D.L. Brain[1], David.Brain@colorado.edu

A.W. Yau[2], yau@phys.ucalgary.ca and

P.G. Richards[3], pgrichds@gmail.com

[1]LASP, University of Colorado, Boulder CO

[2] University of Calgary, Calgary, Alberta, Canada;

[3]George Mason University, Fairfax VA.

Submitted to Advances in Space Research, April 2014.

Abstract: Electron conic distributions have angular distributions with peak fluxes well separated from the field aligned-direction. They have previously been reported at Earth on auroral field lines and at the Moon and Mars on closed crustal magnetic field lines. Here we report observations of electron conics at Earth on closed magnetic field lines well removed from the aurora. We show how these distributions could be produced without plasma wave interactions when magnetic field lines are illuminated by solar ionizing radiation at relatively high altitudes in the ionosphere. Examination of previous reports of electron conic distributions observed in planetary atmospheres show that there are a variety of physical mechanisms that can lead to their formation, not all of which require wave-particle interactions

Highlights: 1) First observations of electron conics well equatorward of the aurora

2) They occur on field lines above shadowed regions of the ionosphere.

3) Acceleration processes are not required to explain the observations.

1.0 Introduction:

Angular distributions of charged particles in the magnetosphere and ionosphere are generally thought of as signatures of plasma energization and acceleration processes. See for example, Shelley [1995]. Particle velocity space distributions peaking along the magnetic field direction are called beams. Conical distributions are characterized by a maximum in an angular distribution well separated from the magnetic field line direction. Operationally, the conic angle is defined as the pitch angle at the flux maximum of the distribution. Ion conic distributions are more well known and have been shown to be the result of plasma heating or energization processes transferring energy to ions in the plane perpendicular to the local magnetic field. See for example, Klumpar et al., [1984], André, [1997], and Collin et al., [1998].

Electron conic distributions are not as well understood and have recently been identified in regions well removed from the Earth's auroral zone. Electron conic distributions may be classified into two distinct types: Uni-directional and bi-directional. Menietti and Burch [1985] first identified uni-directional electron conic distributions appearing as enhancements in the electron flux at pitch angles slightly larger than the loss

cone angle. Burch et al., [1990] showed test particle calculations consistent with observations indicating that bi-directional electron conic distributions are observed on auroral field lines within regions of parallel electron acceleration. André and Eliasson [1992] created a model that demonstrated how low frequency electric fields could produce electron conics. Thompson and Lysak [1996] showed that these low frequency waves arise naturally when Alfvén waves reflect from the ionosphere. Burch [1995] and André [1997] reviewed the extensive set of electron conic observations from multiple platforms and physical mechanisms thought to create them. Both concluded that electron conic distributions were the result of electron acceleration process but that the exact details of the process were not accessible with existing observations and models. Recently, Brain et al., [2007] identified two-sided or bi-directional electron conic distributions in the Martian ionosphere that are not associated with aurora and Halekas et al., [2012] identified electron conics near the Moon..

Here we report uni-directional electron conic distributions on closed magnetic field lines well equatorward of Earth's auroral field lines and compare and contrast them to the electron conic distributions found on closed Martian magnetic field lines. We demonstrate that there are a variety of physical mechanisms that can lead to the formation of electron conic distributions

2.0 Data:

Electron energy spectra from the Fast Auroral SnapshoT (FAST) satellite [Carlson et al., 2001] obtained under conditions of solar illumination (solar zenith angle, SZA < 90^o) equatorward of the auroral field lines have previously been reported by Peterson et al.,

[2008, 2009, and 2012]. Less intense fluxes of photoelectrons are also produced on the nightside of the solar terminator where there is some high altitude illumination when the SZA is larger than 90^o. Figure 1 presents two views of electron energy-angle distributions as a function of time obtained on July 13, 2002 obtained from the FAST spacecraft. During this interval the satellite was at about 3,000 km altitude. The feet of magnetic field lines encountered by FAST in the ionosphere below the satellite were in partial sunlight (SZA > 90^o).

The top panel (Panel A) presents the color-coded energy-time spectrogram of electrons streaming up magnetic field lines with pitch angles within 18^o of the magnetic field direction. Corrections for background noise and varying spacecraft potentials have been applied as described in Peterson et al., [2012]. After about 01:07 the satellite entered the auroral region, which is characterized by rapid changes and more energetic electron distributions. The magnetic footprints of the satellite at 100 km altitude entered full sunlight (SZA < 90^o) conditions after 01:10. Before 01:07:30 the electrons shown in Panel A are produced by photoionization in the ionosphere below the satellite but above the shadow altitude.

Panel B shows angle-time spectrogram of the angular distribution of the electron flux integrated over the five energy bins between 40 and 60 eV in 360^o pitch angle coordinates. For angles less than 180^o the calculated pitch angle is used. For angles above 180^o the angle reported is 360^o minus the calculated pitch angle. In the northern hemisphere, where the data were acquired, photoelectrons near 180^o pitch angle are streaming up magnetic field lines. The horizontal white lines in Panel B indicate 30^o and 150^o pitch angles. Conservation of the first adiabatic invariant requires that, at the

satellite altitude, photoelectrons produced in the 90-180^o pitch angle range in the ionosphere appear in a smaller pitch angle range in the weaker magnetic fields at higher altitudes. This pitch angle range is called the source-cone and includes pitch angles from 150^o to 180^o at the altitudes shown in Figure 1. During the entire interval shown in Figure 1, the spacecraft was in full sunlight and the source-cone angle was greater than 25^o.

The two features appearing at 90^o and 270^o in Panel B are electrons produced on spacecraft surfaces (i.e. spacecraft photoelectrons). After production these electrons orbit the magnetic field and the satellite at pitch angles near 90^o before they are detected. As described in Carlson et al., [2001], data from 32 angular bins are acquired in each accumulation period and then sorted with respect to the magnetic field direction. Because spacecraft photoelectrons are seen over an angular range smaller than the 11.25^o instrumental resolution, the sorting process and finite angular resolution result in apparent shifts in their angular position at ~00:56:30 and ~00:59:15. When the ionosphere is in full sunlight spacecraft generated photoelectrons make a minor contribution to the observed distribution, but they are clearly visible when the flux of ionospheric photoelectrons is weak. As noted above, the energy and angular distributions of electrons change rapidly after ~01:07:30 when the FAST spacecraft entered the auroral zone.

The bottom two panels (Panel C and D) in Figure 1 show the geometrical shadow altitude of the sun and the solar zenith angle (SZA), respectively, on the field line below the satellite as a function of time. During this interval, FAST is on magnetic field lines behind the solar termination line; the SZA at the magnetic foot point below the satellite is greater than 90^o and the SZA at the magnetic conjugate foot point in the southern hemisphere is greater than 120^o. Before ~00:59 FAST was on field lines that were in the

Earth's shadow at altitudes below 330 km. The increase in flux of photoelectrons starting at this time in Panel A corresponds to the decreasing shadow altitude and the correspondingly increasing altitude region of photoelectron production. The flux of upflowing photoelectrons is relatively constant after 01:05 where the shadow altitude is 140 km and the SZA is 95^{o}.

Electron conic distributions can be clearly seen in Panel B at time before 01:00 as intensifications near the source-cone angle. Figure 2 shows line plots of the pitch angle distributions of the integrated flux in this panel. Data taken at various times are identified by letter and shown in different colors and styles. The black dotted lines (labeled A) on the bottom are spectra obtained before 00:59, when the solar zenith angle was greater than 101^{o} and the EUV shadow altitude (along the field line) was below the satellite and above 330 km. The prominent peaks near 90^{o} and 270^{o} are photoelectrons generated on the spacecraft surface. Electron conic distributions are seen as relative peaks near 150^{o} and 210^{o}. We note that these electron conic distributions are seen well equatorward of the auroral region.

The dotted green lines (labeled B) show data between 01:06:00 and 01:06:30, when the shadow height was between 110 and 120 km. The ionospheric source-cone is now filled with upflowing electrons created by photoionization in the ionosphere below. One side of the spacecraft is more strongly illuminated during this interval leading to the asymmetry in the spacecraft generated photoelectron signals between ~90^{o} and 270^{o}. The integrated flux during this interval is quasi-isotropic with the notable exceptions of 1) the source cone population (~150^{o} to ~210^{o}), 2) spacecraft generated photoelectrons near 90^{o} and 270^{o}, and 3) electrons at angles below 30^{o} and above 330^{o}. The quasi-isotropic

distribution is the result of electrons scattering out of the source cone as they bounce between hemispheres; the relative minimum in flux below 30^o and above 330^o is the result of losses to the atmosphere at the conjugate magnetic foot point.

The solid black lines (labeled C) show data between 01:08:51 and 01:08:54, when the satellite was on auroral field lines and the magnetic field intensity was about 3,000 nT at the satellite altitude. The characteristic electron gyro radius of the 40-60 eV electrons here is ~ 5 m, which is comparable to the spacecraft dimensions. The one angular bin wide relative minima near 90^o and 270^o in the solid black lines is the result of a small fraction of electrons near 90^o pitch angle being shielded from detection by the spacecraft. The angular range of the shielding decreases with increasing electron energies.

Figure 3 provides line plots of selected electron conic distributions observed before 01:02. The format is the same as in Figure 2. Table 1 gives the UT time of observation, shadow height, solar zenith angle (SZA) at the magnetic foot point, ratio of the integral flux in the middle of the loss cone to that at the edge, an estimate of the fraction of the electrons at the edge of the loss cone that have mirrored below the satellite, and color for 6 selected angular distributions shown in Figure 3. During this interval photoelectrons produced on the field line below the spacecraft and above the shadow height follow one of two independent paths to the detector: A) electrons produced in the upward hemisphere proceed directly to the satellite and uniformly fill the source-cone; B) electrons produced in the downward hemisphere either mirror or are absorbed by the atmosphere below the point where they are produced. These electrons will have a distribution with a minimum along the field line and a maximum at the source-cone angle. The ratio shown in Table 1 is the ratio of the upward flux at the center of the source-cone

to the average of the upward flux at the edges of the source-cone. The fraction of the upflowing flux at the edge of the loss cone that has mirrored below the satellite can be calculated from this ratio and is reported in Table 1. The 30-40% mirrored flux for the highest shadow heights for 40-60 eV electrons is consistent with the electron reflection coefficients reported by Richards and Peterson [2008].

The observations presented above are also consistent with those obtained from photoelectron production codes. Figure 4 presents the results obtained from the Field Line Inter-hemispheric Plasma (FLIP) code [Richards et al., 2001] for 300, 500, and 700 km altitudes on field lines below the FAST satellite for the times indicated. Data are presented for number fluxes between 40 and 60 eV. Upward directed fluxes are indicated by solid lines and downward directed fluxes by dotted lines. The upward directed fluxes appearing at 300 km (black lines) are less intense than the downward fluxes for all times shown in Figure 4, reflecting the fact that the peak of the photoelectron production region is above 300 km for this interval. The main photoelectron production region is below 500 km as shown by the ratio of upward to downward fluxes at 500 (green) and 700 (red) km. It is not possible to use the FLIP code to calculate the parameters given in Table 1 because the FLIP code is a two-stream code, so it provides no information about pitch angle distributions.

3.0 Discussion:

Electron and ion angular and energy distributions observed in space plasmas are interesting because they provide insights into the processes that create them. Two distinctly different types of auroral electron conic distribution have been reported: Uni-

directional and bi-directional. At Earth both types have been reported on auroral field lines (e.g., Burch, 1995). At the Moon only uni-directional conics have been reported (e.g. Halekas et al, 2012). At Mars only bi-directional electron conics have been reported (e.g., Brain et al., 2007). Observations of electron energy and angular spectra from rockets and satellites at Earth have been made since the beginnings of the space age. It is therefore surprising that, to our knowledge, this is the first report of uni-directional electron conic distributions on closed magnetic field lines well removed from Earth's aurora. Here we compare and contrast them with electron conic distributions observed on closed Martian magnetic field lines.

On auroral field lines, it is generally agreed that uni-directional electron conic distributions are produced when electrons are accelerated downward into the ionosphere and subsequently reflected by the magnetic mirror force associated with the conservation of the first adiabatic invariant (Burch 1995, André, 1997). The deeper penetration of the near field aligned component of precipitating electrons and their correspondingly greater loss into the ionosphere lead to the more effective reflection of electrons near the loss cone angle and subsequent enhancement of the upward flux of electrons at the edges of the loss cone. Here we have shown that this mechanism also works on field lines where no electron and plasma wave interaction acceleration mechanisms are active. The electron conic distributions reported in Figures 1-4 are fully consistent with photoelectron production at relatively high altitudes (i.e. greater than 300 km) on magnetic field lines above the shadow altitude, in the absence of acceleration or energization. The conic "wings" that appear near the electron source cone are the result of photoelectrons mirroring below their production altitude.

Uni-directional electron conic distributions on closed field lines equatorward of the auroral zone are regularly observed when the solar illumination and magnetic field line configuration meet two conditions. The first condition is that the ionosphere below ~ 300 km be in darkness while it is sunlit above. The second condition is that both feet of the magnetic field line must be in darkness (SZA > 90^o). If the local or magnetically conjugate foot point is sunlit (SZA < 90^o) then the flux of photoelectrons produced above 300 km and reflected from the ionosphere below will be small compared to the other components and the conic signature will be too small to be detectable. These conditions occur most frequently near the summer and winter solstices on magnetic field lines with significant east-west components at the equator allowing darkness at both ends.

On Mars, aurorae occur less frequently and over a smaller volume than on Earth [Bertaux et al., 2005]. Because of the small size and rapid velocity of platforms carrying electron and ion spectrometers at Mars, direct observations of charged particle distributions on Martian auroral field lines are scarce. Those distributions that exist show signatures of electron and ion acceleration processes [e.g., Dubinin et al., 2008, Brain et al., 2006, Lundin et al., 2006]. Table 1 of Brain et al., [2007] notes that unidirectional electron conics occur on Mars.

The bi-directional electron conics observed at Mars and described in Brain et al., [2007] and further investigated by Ulusen et al., [2011] appear to be fundamentally different than the bi-directional conics seen at Earth reported by Burch et al., [1990]. At Mars they appear only on closed magnetic field lines well removed from the open and closed field line boundaries. These distributions have been found occasionally in full sunlight (~15% for SZA < 60^o) and near the terminator (~25% for 60^o < SZA < 120^o) but

primarily in full darkness (~60% for SZA > 120^{o}) in the Mars Global Surveyor (MGS) Electron Reflectometer (ER) data analyzed by Ulusen et al., [2011]. These investigators were unable to determine if the high occurrence rate in full darkness was real or the result of reduced dayside detection efficiency caused by high fluxes of isotropic photoelectrons on the dayside at the MGS altitude. Electron kinetic properties suggest that the bi-directional conics are produced on the night side of Mars, and are not transported from the dayside. The mechanisms producing these bi-directional electron conic distributions on Mars are not fully understood. Two mechanisms for production have been proposed: 1) Addition of plasma to closed field lines by reconnection and subsequent preferential loss for electrons with pitch angles near 90^{o} [Brain et al., 2007], and 2) Diffusion of plasma onto closed field lines in the collision dominated region of the ionosphere [Ulusen et al., 2011]. The limitations of the MGS/ER data preclude the definitive identification of the processes responsible for the Martian bi-directional electron conics.

There are no observations of bi-directional electron conics on closed, non-auroral, field lines at Earth. There are, however, reports of bi-directional ion conic distributions on closed field lines at Earth. Nagai, et al., [1983] and Sagawa et al., [1987] reported bi-directional ion distributions on closed field lines near and equtorward of the auroral zone with morphology similar to the bi-directional electron distributions seen at Mars. These ion distributions are seen in both H^{+} and O^{+} ions primarily on the dawn side of the magnetosphere on auroral field lines. Broad bi-directional ion beams (counter streaming ions, CSI in the Sagawa et al. terminology) were reported on the same field lines as bi-directional conics, but at earlier local times. Sagawa et al., [1987] argued that bi-directional ion conics evolved from the CSI as a result of the slow eastward drift of the

ions and the preferential charge exchange in the field aligned directions with neutral hydrogen atoms. Our results suggest that a pitch angle dependence of ions reflecting off of the ionosphere could also lead to bi-directional ion conics. Sagawa et al. [1987] noted that the small occurrence of bi-direction ion conics in the post noon sector cannot be explained by losses in the field-aligned direction only.

Because of the similarities of the morphology of the bi-directional ion conics on closed field lines at Earth and the bi-directional electron conics found on closed Martian crustal magnetic field lines we suggest that some form of wave/particle interaction is active at Mars that preferentially removes electrons near 90^{o} pitch angles as suggested by Brain et al., [2007]. It is fortunate that there will soon be a full plasma wave and particle package at Mars that will be able to provide more insight into processes responsible for the formation of bi-directional electron conics.

4.0 Conclusions:

To our knowledge, this is the first report of electron conic distributions on closed magnetic field lines well separated from magnetic field lines associated with the Earth's aurora. We showed how these distributions could naturally be formed by photoionization at relatively high altitudes on shadowed magnetic field lines followed by reflection or absorption in the ionosphere below without involving any plasma wave interactions and/or acceleration processes. As noted by Halekas et al., [2012], electron conic distributions recently reported upstream from the Moon appear to require more than kinematic processes for formation.

The creation of Martian bi-directional electron conic distributions on closed magnetic field lines cannot be explained by simple photoionization on shadowed magnetic field lines. Using the analogy of bi-directional ion conics on closed magnetic field lines at Earth suggests that plasma wave interactions are required to remove electrons near 90^o pitch angles and form the bi-directional conics as suggested by Brain et al., [2007].

We conclude that there are a variety of physical mechanisms that can lead to the formation of electron conic distributions in planetary atmospheres, not all of which require wave-particle interactions.

Acknowledgements:

W.K.P. was supported by NASA Grant NNX12AD25G

References:

André, M, and L. Eliasson (1992), Electron acceleration by low frequency electric field fluctuations: Electron conics, Geophys. Res. Lett. 19, 1073.

André, M. (1997), Waves and wave-particle interactions in the aurora1 region, J. Atmos. and Solar Terr. Phys. 59, 1687.

Bertaux, J. L., F. Leblanc, O. Witasse, E. Quemerais, J. Lilensten, A. S. Stern, B. Sandel, and O. Korablev (2005), Discovery of aurora on Mars, Nature, 435, 790–794, doi:10.1038/nature03603.

Brain, D. A., F. Bagenal, M. H. Acuña, and J. E. P. Connerney (2003), Martian magnetic morphology: Contributions from the solar wind and crust, J. Geophys. Res., 108, 1424, doi:10.1029/2002JA009482, A12.

Brain, D. A., J. S. Halekas, L. M. Peticolas, R. P. Lin, J. G. Luhmann, D. L. Mitchell, G. T. Delory, S. W. Bougher, M. H. Acuña, and H. Reme (2006), On the origin of aurorae on Mars, Geophys. Res. Lett., 33, L01201, doi:10.1029/2005GL024782.

Brain, D. A., R. J. Lillis, D. L. Mitchell, J. S. Halekas, *and* R. P. Lin *(*2007*),* Electron pitch angle distributions as indicators of magnetic field topology near Mars, J. Geophys. Res., 112, *A09201, doi:*10.1029/2007JA012435.

Burch, J.L., C. Gurgiolo, and J. D. Menietti (1990), The electron signature of parallel electric fields, Geophys. Res. Lett. 17, 2329.

Burch, J.L. (1995), Dynamics Explorer observations of the production of electron conics, Geophys. Res. Lett. 22, 2705, doi: 10.1029/95GL02817

Carlson, C. W., et al. (2001), The electron and ion plasma experiment for FAST, *Space Sci. Rev.*, 98, 33.

Collin, H.L., W.K. Peterson, O.W. Lennartsson, and J.F. Drake (1998), The seasonal variation of auroral ion beams (1998), Geophys. Res. Lett., 25, 4071, doi: 10.1029/1998GL900090

Dubinin, E. M., M. Fraenz, J. Woch, E. Roussos, J. D. Winningham, R. A. Frahm, A. Coates, F. Leblanc, R. Lundin, and S. Barabash (2008), Access of solar wind electrons into the Martian magnetosphere, Ann. Geophys., 26(11), 3511–3524, doi:10.5194/angeo-26-3511-2008.

Halekas, J.S., A. Poppe G.T. Delory, W.M. Farrell, and M. Horányi (2012), Solar wind electron interaction with the dayside lunar surface and crustal magnetic fields: Evidence for precursor effects, Earth Planets Space, 64, 73, doi:10.5047/eps.2011.03.0008

Klumpar, D. M., W. K. Peterson, and E. G. Shelley (1984), Direct evidence for two-stage (bimodal) acceleration of ionospheric ions, J. Geophys. Res., 89(A12), 10779–10787, doi:10.1029/JA089iA12p10779.

Nagai, T., J. F. E. Johnson, and C. R. Chappell, Low-energy (<100 eV) ion pitch angle distributions in the magnetosphere by ISEE 1, J. Geophys. Res., 88, 6944, 1983.

Lundin, R., et al. (2006), Plasma acceleration above Martian magnetic anomalies, Science, 311, 980–983, doi:10.1126/science.1122071.

Menietti, J. D., and J. L. Burch (1985), "Electron conic" signatures observed in the nightside auroral zone and over the polar cap, J. Geophys. Res., 90(A6), 5345–5353, doi:10.1029/JA090iA06p05345.

Peterson, W.K., P.C. Chamberlin, T.N. Woods, and P.G. Richards (2008). Temporal and spectral variations of the photoelectron flux and solar irradiance during an X class solar flare, *Geophys. Res. Lett.*, 35, L12102, doi: 10.1029/2008GL033746.

Peterson, W.K., E.N. Stavros, P.G. Richards, P.C. Chamberlin, T.N. Woods, S.M. Bailey, and S.C. Solomon (2009), Photoelectrons as a tool to evaluate spectral variations in solar EUV irradiance over solar cycle time scales, *J. Geophys. Res.,* 114, A10304, doi:10.1029/2009JA014362.

Peterson, W. K., T. N. Woods, J. M. Fontenla, P. G. Richards, P. C. Chamberlin, S. C. Solomon, W. K. Tobiska, and H. P. Warren (2012), Solar EUV and XUV energy input to thermosphere on solar rotation time scales derived from photoelectron observations, *J. Geophys. Res.*, *117*, A05320, doi:10.1029/2011JA017382.

Richards, P. G. (2001), Seasonal and solar cycle variations of the ionospheric peak electron density: Comparison of measurement and models, J. Geophys. Res., 106, 12,803, doi:10.1029/2000JA000365.

Richards, P. G., and W. K. Peterson (2008), Measured and modeled backscatter of ionospheric photoelectron fluxes, J. Geophys. Res., 113, A08321, doi:10.1029/2008JA013092.

Sagawa, E., A. W. Yau, B. A. Whalen, and W. K. Peterson (1987), Pitch angle distributions of low-energy ions in the near-Earth magnetosphere, J. Geophys. Res., 92(A11), 12241–12254, doi:10.1029/JA092iA11p12241.

Shelley, E. G. (1995), The auroral acceleration region: The world of beams, conies, cavitons, and other plasma exotica, Rev. Geophys., 33(S1), 709–714, doi:10.1029/95RG00253.

Thompson, B.J. and R.L. Lysak (1996), Electron acceleration by inertial Alfven waves, J. Geophys. Res., 103(A3), 5359-5369

Ulusen, D., D. A. Brain, *and* D. L. Mitchell *(*2011*),* Observation of conical electron distributions over Martian crustal magnetic fields, J. Geophys. Res., 116, *A07214, doi:*10.1029/2010JA016217.

UT	Shadow height (km)	SZA (degrees)	Ratio	Fraction mirrored	Color in Figure 3
00:57	424	103	.75	.33	Black
00:58	374	102	.72	.38	Red
00:59	332	101	.80	.24	Green
01:00	290	100	.79	.26	Orange
01:02	223	98	.95	.05	Blue

Table 1. Parameters relating to the data shown in Figures 1, 2, and 3. See text.

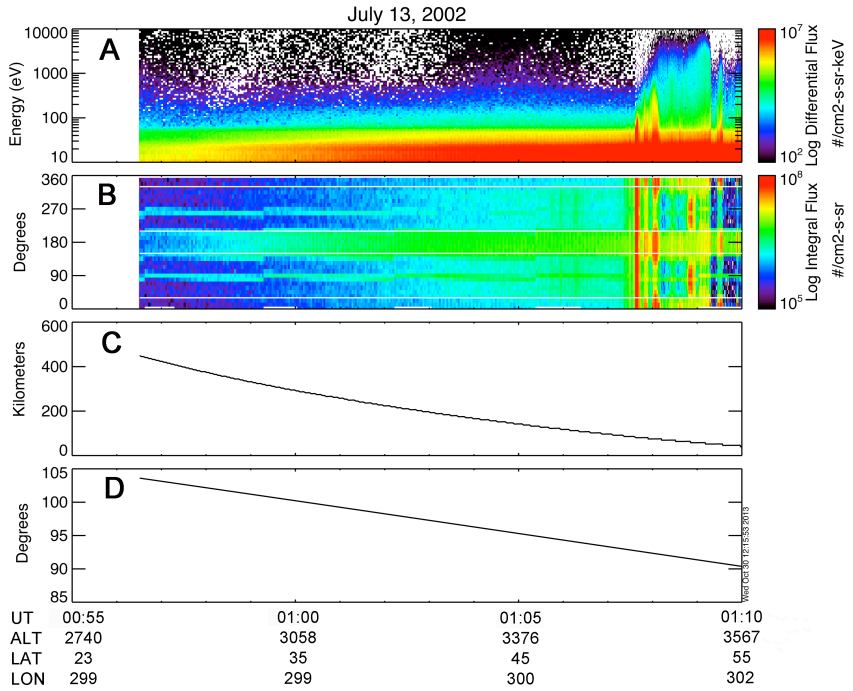

Figure 1. Data obtained on July 13, 2002. The satellite position in altitude (ALT), latitude (LAT) and longitude (LON) for several universal times (UT) is show at the bottom. A) Energy-time spectrogram of the differential number flux of upflowing photoelectrons from the ionosphere below encoded in units of $(cm^2\text{-s-sr-keV})^{-1}$ shown in the color bar.. B) Angle-time spectrogram of the flux of electrons integrated over the 40 to 60 eV range encoded in units of $(cm^2\text{-s-sr})^{-1}$ shown in the color bar. C) The geometrical shadow altitude of the sun on the magnetic field line below the satellite. D) The solar zenith angle at the magnetic conjugate point in the ionosphere below the satellite. See text.

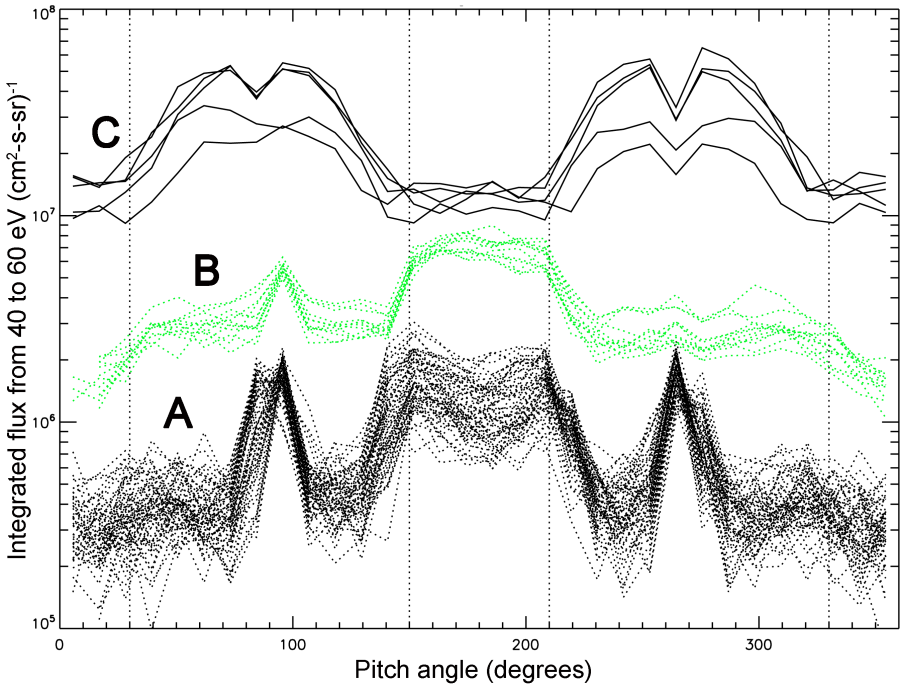

Figure 2. Line spectra of the intensity of integrated angular distribution of electron number flux integrated over 40-60 eV before 01:00 (A), at 01:06:00 to 01:06:30 (B), and at 01:08:51 to 01:08:54 (C). See Text.

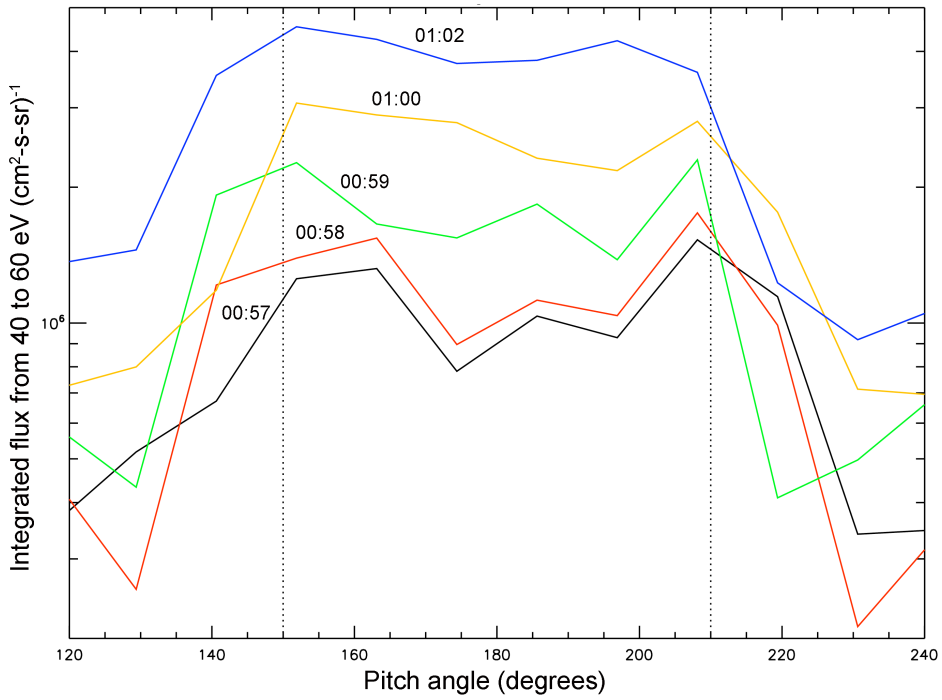

Figure 3: Selected pitch angle distributions from Figure 2 shown with higher angular resolution.

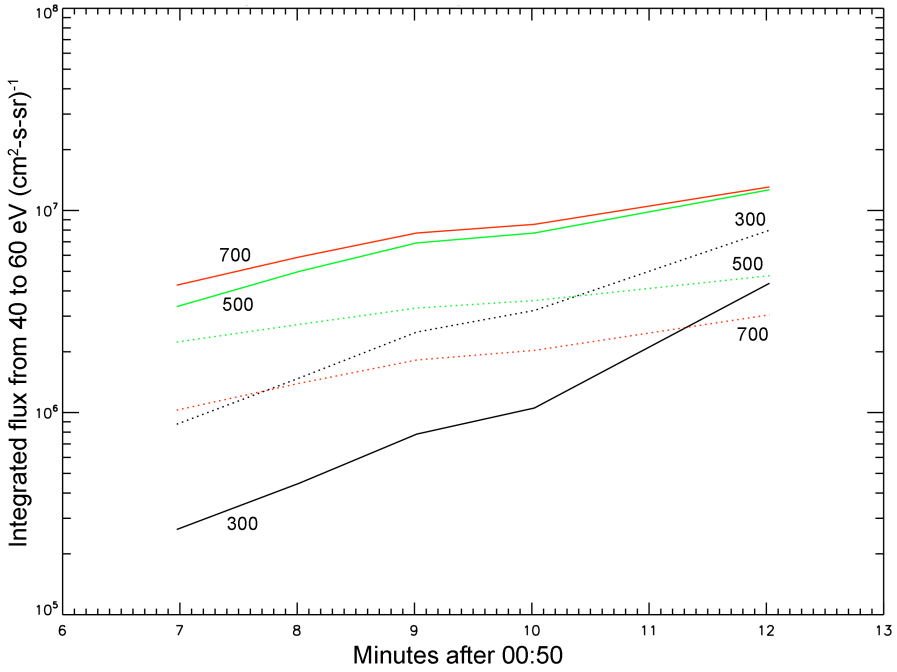

Figure 4. Modeled upward (solid) and downward (dotted) photoelectron flux in the 40 to 60 eV range at the indicated altitudes on field lines below the FAST satellite for the indicated times. See text.